RSC Advances

PAPER

View Article Online
View Journal | View Issue

Cite this: *RSC Adv.*, 2017, **7**, 10235

Solvent co-mediated synthesis of ultrathin BiOCl nanosheets with highly efficient visible-light photocatalytic activity†

Xiaoyu Li,[ab] Chengzhou Zhu,[a] Yang Song,[a] Dan Du[a] and Yuehe Lin*[a]

Received 1st December 2016
Accepted 25th January 2017

DOI: 10.1039/c6ra27606g

rsc.li/rsc-advances

A series of bismuth oxychloride (BiOCl) nanostructures were prepared *via* a facile solvothermal method. Well-crystallized BiOCl nanosheets were successfully obtained by controlling the ratio of different solvents. With an optimal volume ratio of solvents, sodium chloride (NaCl) and cetyltrimethylammonium chloride (CTAC) were chosen to provide the chloride sources, separately. Compared with NaCl, besides acting as one kind of chloride source, it was found that CTAC could play a significant role in controlling the square-like structure of BiOCl. In addition, the obtained ultrathin square-like BiOCl nanosheets with 3–7 nm thickness exhibited high activity for rhodamine B (RhB) photosensitization degradation under visible-light irradiation. The BiOCl nanosheets synthesized from this study had large surface areas from 20 $m^2\ g^{-1}$ to 35 $m^2\ g^{-1}$, which are favorable for providing more active sites for dye adsorption and degradation. The possible mechanisms of crystal growth and degradation for RhB are discussed.

1. Introduction

In recent decades, due to increasing exploitation and use of fossil fuels, human beings need to confront the crisis of environmental pollution, such as water pollution and air pollution. Researchers are trying to exploit new methods and alternative energy to solve environmental pollution problems. Among them, photocatalysis has been considered as a prompt and important way for decomposing organic pollutants and producing hydrogen energy *via* light irradiation.[1–4] In this way, organic pollutants may be degraded into non-hazardous compounds such as water, carbon dioxide and other non-toxic small molecules. Due to the wide band gap of the conventional TiO_2 (P25) photocatalyst,[5] P25 only responds to ultraviolet (UV) light which merely occupies 4% of sunlight energy. Because visible light occupies about 49% of sunlight energy, great efforts have been made to take full advantage of solar energy and explore diverse, novel photocatalysts working under visible-light irradiation. Bismuth oxychloride (BiOCl), as a promising candidate for Bi-based semiconductors, has great potential in photocatalysis applications. Besides its good performance under UV light irradiation, BiOCl nanomaterials also exhibits superior efficiency in visible-light photocatalysis. This feature flourishing in various applications currently draws a large amount of attention.[6–11]

The photocatalytic property of the BiOCl semiconductor closely relies on morphologies and structures.[6,7,11] Two-dimensional (2D) nanostructures are of great significance due to outstanding catalytic and optical properties, as well as potential uses for building novel 3D structure and advanced devices.[9] Great attention has been paid to 2D nanostructures, which include nanosheets, nanoplates and nanoflakes.[8–14] The lamellar structure with high crystallinity may reduce the recombination opportunities of charge carriers. Additionally, the surface specific area increased dramatically with decreasing of material size. In this case, the efficiency of organic pollutants' photodegradation improves tremendously due to more effective electron surface transformation. However, few uniform ultrathin nanosheets of BiOCl materials with highly efficient visible-light-driven activity have been reported. It has been widely reported that polyols can act as general reducing agents when preparing with metal and metal oxide.[15,16] The solvothermal synthesis assisted by polyols is one of the most common methods when preparing BiOX (X = Cl, Br, I) nanomaterials. These are, for example, ethylene glycol (EG),[17–19] diethylene glycol (DEG),[20,21] glycerol,[22,23] triethylene glycol (TEG)[24,25] and mannitol.[8,9] To better control particle growth, EG is often chosen to serve as high-boiling solvent and stabilizer.[17,26] Its highly polar, ionic intermediates and strong chelating ability fascinate the process of complex formation with transition metal ions by using hydroxyls as ligands.[17] Zhang's group stated that EG plays an important role in the formation of hierarchical BiOX nanoplate microspheres.[17] Recently, it also has been reported that mannitol may lead to morphology of regular square-like nanoplates because it can adsorb on a specific plane of BiOCl nuclei and efficiently restricting anisotropic growth.[9] Dr

[a]*School of Mechanical and Material Engineering, Washington State University, Pullman, Washington 99163, USA. E-mail: yuehe.lin@wsu.edu*

[b]*Department of Civil, Environmental and Geomatics Engineering, Florida Atlantic University, Boca Raton, Florida 33431, USA*

† Electronic Supplementary Information (ESI) available: Fig. S1(a) the low magnification SEM image of BiOCl microsphere (S1) and (b–d) chemical element mapping images. See DOI: 10.1039/c6ra27606g

Chen's group reported tunable BiOCl nanostructures *via* controlling different polyols as solvents, however, further research on polyols' roles and co-mediated studies are essential to be done. While many reports discuss the synthesis of BiOCl nanostructures with a single solvent, few researchers focus on the significance of polyols co-mediated preparation.

In this study, well-crystallized BiOCl nanosheets were synthesized *via* a facile, modified solvothermal method. We focused on a polyols co-mediated preparation mechanism and gained optimal volume ratio between mannitol and EG. On one hand, the thickness of BiOCl nanosheets was tuned by solvent ratio. On the other hand, the morphology and thickness of BiOCl nanosheets could be controlled with different amount of Cl sources. Different morphology, texture and catalytic efficiencies of samples by using different Cl sources were discussed. We obtained 3–7 nm square-like ultrathin BiOCl nanosheets that showed outstanding visible-light photocatalytic activity. Compared with commercial BiOCl powder, the BET surface areas of our ultrathin nanosheets were at least 100 times larger than commercial one (0.2 $m^2\ g^{-1}$). As expected, larger specific area could provide many active sites and large adsorption capacity. The photodegradation efficiency of BiOCl nanosheets for rhodamine B (RhB) was investigated and a proposed mechanism is discussed.

2. Experimental

2.1. Materials

All chemicals used in this work were purchased from Sigma-Aldrich Company, USA. All reagents for this study are analytical standard and used without further purification. Double distilled water was used in all the experiments whenever required.

2.2. Preparation of the ultrathin BiOCl nanosheets

The preparation of ultrathin BiOCl nanosheets was based on a modified solvothermal method.[8] Typically, 0.486 g $Bi(NO_3)_3 \cdot 5H_2O$ (1 mM) was dissolved in 10 mL of 0.5 M mannitol solution with 15 min vigorous stirring. A certain amount of NaCl powder was dissolved in 10 mL EG solution. Then NaCl solution as a Cl source was slowly dropped into Bi source solution with continuous stirring to produce a white suspension. After reacting for 20 min, the solution was transferred into an 80 mL Teflon-lined stainless steel autoclave and underwent a solvothermal process at 140 °C for 24 h. After that, the autoclave was permitted to cool down to room temperature naturally. The products were then obtained after washing with ethanol and water for 3 times, respectively. In this way, the possible remaining impurity was removed. The final products were collected and dried in vacuum at 70 °C for 2 h for future characterization. This is a typical procedure and other samples were synthesized under the identical conditions by changing the solvent ratios or Cl sources. The conditions of sample synthesis are demonstrated in Table 1.

Table 1 BiOCl nanosheets samples synthesized in different conditions

Sample	$V_M : V_E$	$Bi(NO_3)_3 \cdot 5H_2O$ (mM)	NaCl (mM)	CTAC (mM)
1	1 : 3	1	1	—
2	1 : 1	1	1	—
3	3 : 1	1	1	—
4	1 : 1	1	Saturated	—
5	1 : 1	1	—	25
6	1 : 1	1	—	50
7	1 : 1	1	—	100
8	1 : 1	1	—	150

2.3. Physicochemical characterization of samples

X-ray powder diffraction (XRD) characterization was carried out at a scan rate of 5° min^{-1} in the 2θ degree range from 10° to 70° by a Rigaku Miniflex 600. It is a useful analytical technique that is used in the field of phase identification and for finding unit cell dimensions of crystalline materials. Scan electron microscopy (SEM) images were tested by a Robinson Model RBH57OR Microscope, which was connected to energy dispersive spectrum analysis system (EDS). Transmission electron microscopy (TEM) images were taken on a Philips CM200UT microscope. The Brunauer–Emmett–Teller (BET) analysis was conducted on a TriStar II 3020 Automatic Physisorption Analyzer to measure the specific surface area of the sample powders. Atomic force microscope (AFM) images were obtained by a Bruker FastScan AFM. All tests of photodegradation results were performed using a Thermo Scientific Evolution 300 UV-vis spectrometer. The photocatalytic machine 71SC5 was purchased from SOFN Instruments Co., LTD.

2.4. Measurements of photocatalysis

The visible-light-driven photocatalytic activities of the BiOCl nanostructures were conducted by the degradation of a certain concentration of RhB solution. A 300 W Xe lamp was used as the light source. To guarantee the irradiation was from visible light, a 420 nm cutoff filter was chosen and put in front of light pathway tube. The reaction cell was put into a sealed black box and in front of the light irradiation. In every experiment, 10 mg BiOCl photocatalysts were used to degrade 20 mL 10 mg L^{-1} RhB solution. Prior to light irradiation, the suspensions were stirred in the dark for half an hour. This process was designed to attain the equilibrium of adsorption–desorption. After that, the suspension was exposed to visible-light irradiation with continuous stirring. 2 mL samples of the suspensions were taken at 5 min interval until the solution became colorless. All slurry samples were centrifuged (6000 rpm, 5 min) in order to remove BiOCl photocatalyst particles.

3. Results and discussion

3.1. Mechanism of crystal growth

In our experiments, mannitol and EG, as two kinds of main solvents, play important roles in controlling nanostructures of BiOCl. Without the presence of surfactants, we predicted that these two kinds of polyols could co-mediate to prepare BiOCl nanomaterials. The volume ratio of mannitol and EG is crucial for formation of uniform ultrathin nanosheets. Scheme 1

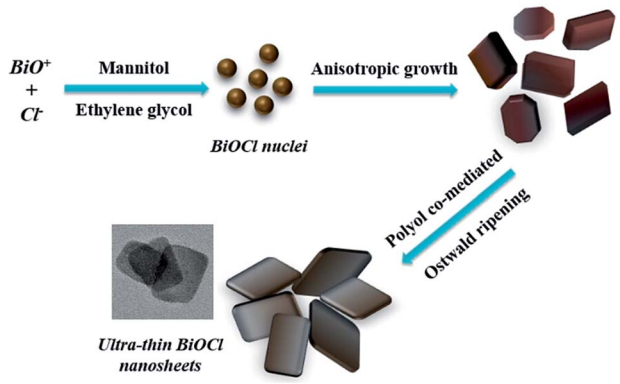

Scheme 1 Schematic illustration of ultrathin BiOCl nanosheets formation.

demonstrates the formation of BiOCl nanosheets under polyol co-mediated conditions. It is well known that there are two necessary steps to form crystal nanostructures: (1) nucleation; (2) growth.[27] At the very beginning, with large amounts of BiO^+ ions present, the reactants are added into the reaction system and many BiOCl nuclei form in a short period. Because of the intrinsic special structure of BiOCl crystals,[6,28] these nuclei anisotropically grow into 2D nanostructures. Subsequently, random shaped BiOCl nanosheets continue to grow and may self-assemble with the control of polyols. As reaction time increased, the nuclei continue to grow and ultrathin BiOCl nanosheets are synthesized successfully. According to crystal habit, the growth procedure was developed based on the effect of exposed facets energy.[27,29] The solvents and reagents can indirectly affect the surface energy. Here, polyhydroxyl of mannitol molecules will absorb on top-bottom facets and change surface energy.[9] Thus, the energy of side facets is larger than top-bottom facets, which results in growing in certain directions to form a square-like nanostructure.

3.2. Solvents co-mediated synthesis with NaCl as Cl source

Large quantities of BiOCl quadrilateral nanosheets were obtained *via* this solvothermal method. Fig. S1(a–d)† shows the chemical element mapping analysis. It is found that bismuth, oxygen and chloride are homogenously distributed over the sample. The TEM images of BiOCl reveal that nanosheets in different width and thickness were synthesized in different volume ratios of mannitol and EG. For convenience, the volume of mannitol and EG are written in short for V_M and V_E, respectively. When V_E is larger than V_M, EG-induced self-assembly[17] of nanosheets occurs. The BiOCl nanoparticles aggregate and form regular hierarchical microspheres (Fig. S1a† and 1a, $V_M : V_E = 1 : 3$). On the contrary, as the ratio of $V_M : V_E$ increases until there is equal, then more, mannitol than EG, BiOCl nanosheets do not have the potential to aggregate into microspheres to form a 3D architecture any more. With increasing ratio of $V_M : V_E$, S2 (Fig. 1b, $V_M : V_E = 1 : 1$) and S3 (Fig. 1c, $V_M : V_E = 3 : 1$), BiOCl does not come into being hierarchical microstructure assembled with nanosheets. The comparison of width distribution and thickness range of the as-synthesized

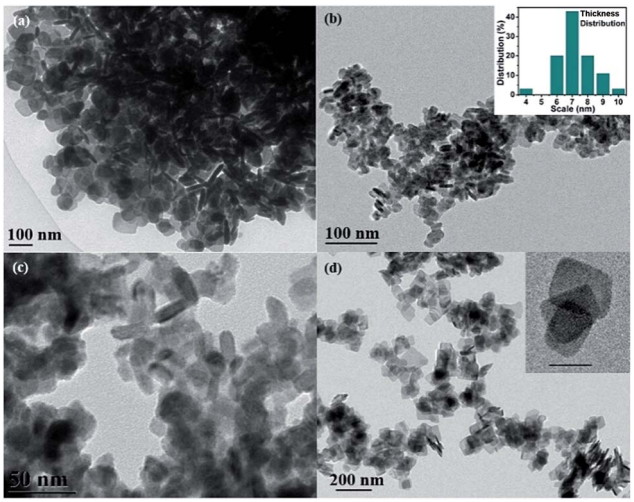

Fig. 1 (a–d) Typical TEM images of BiOCl nanosheets S1–S4 prepared by solvothermal method with NaCl as Cl sources under different volume ratios of mannitol to EG. Insert pictures are thickness distribution (b) and large magnification of TEM image with scale bar 20 nm (d).

samples 1–8 were collected in Table 2. As can be seen, the products are plate-like in shape with different sizes and thickness. S2 (Fig. 1b, $V_M : V_E = 1 : 1$) has the smallest thickness as well as narrow thickness distribution from 3 nm to 11 nm, which was shown in the inserted chart. Compared with S1 and S3, S2 exhibits uniform thickness distribution and the smallest average thickness. Thus, we proposed that 1 : 1 is the optimal ratio between these two solvents. To investigate the effect of Cl source concentration, controlled experiments were conducted under saturated NaCl solution. S4 was prepared under the optimal ratio when other parameters were kept the same except Cl source concentration. The results indicate that the morphology of nanosheets tend to be square-like and size increases dramatically (Fig. 1d). Therefore, under the condition of higher Cl source concentration, the width of nanosheets grow rapidly and thickness increases to a large degree.

3.3. Solvents co-mediated synthesis with CTAC as Cl source

Based on the above discussion, the amount of Cl source from NaCl is proposed to have a significant influence on BiOCl crystal

Table 2 Results and comparisons of different BiOCl samples

Sample	Thickness (nm)	Width (nm)
S1 (Fig. 1a)	10–25	45–88
S2 (Fig. 1b)	4–11	14–22
S3 (Fig. 1c)	8–12	11–22
S4 (Fig. 1d)	9–18	38–120
S5 (Fig. 2a)	3–5	21–42
S6 (Fig. 2b)	3–5	10–14
S7 (Fig. 2c)	3–7	17–35
S8 (Fig. 2d)	6–13	27–72

growth. Besides NaCl is regarded as one of the common Cl sources, surfactant CTAC could act as another ideal candidate when preparing BiOCl nanosheets.[30] It is worthwhile to mention that CTAC serves as both Cl source and soft template.[30] Unlike NaCl, the Cl ions release rate of CTAC are very slow. During the preparation process, dissolved Bi^{3+} reacts with CTAC and produces the complex of $C_{16}H_{33}(CH_3)_3N$–Cl and Bi^{3+}.[31] Subsequently, the BiOCl nucleates and grows anisotropically under the solvothermal atmosphere. Reaction details are shown in below formula:

$$Bi(NO_3) \rightarrow Bi^{3+} + 3NO_3^-$$

$$Bi^{3+} + C_{16}H_{33}(CH_3)_3N\text{–}Cl \rightarrow C_{16}H_{33}(CH_3)_3N\text{–}Cl\text{–}Bi^{3+}$$

$$C_{16}H_{33}(CH_3)_3N\text{–}Cl\text{–}Bi^{3+} + H_2O \xrightarrow{\text{solvent-thermal}} BiOCl + C_{16}H_{33}(CH_3)_3N^+ + 2H^+$$

Under the condition of an optimal volume ratio of EG and mannitol, the agglomeration of BiOCl nanosheets could be significantly inhibited upon addition of CTAC. To further study the role of CTAC, S5–S8 were prepared under the same parameters except the amount of CTAC. From TEM images in Fig. 2a–d, all BiOCl samples exhibit lamellar-like nanostructures. Sample 7, which was synthesized with optimal amount of CTAC (when the amount ratio of Bi and Cl is about 1 : 1), shows uniform square-like nanosheets and explicit edges (Fig. 2c). It also has the smallest thickness as well as narrow thickness distribution from 3 nm to 7 nm, which is shown in inserted chart. AFM image and its corresponding height profiles (Fig. 3) demonstrates that the average thickness values of ultrathin BiOCl nanosheets of S7 was 3.5 nm, which matches very well

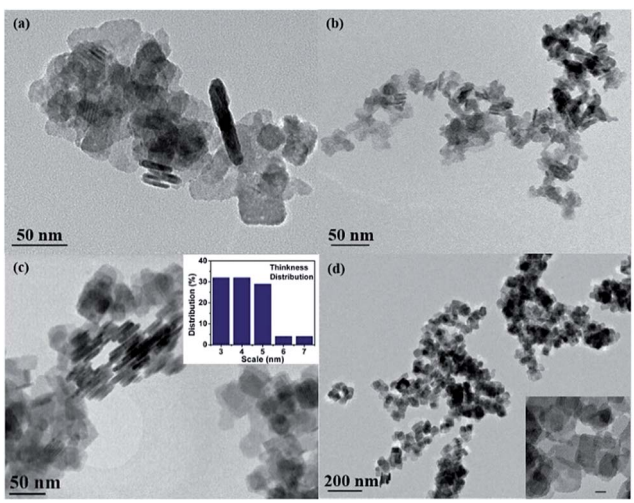

Fig. 2 (a–d) Typical TEM images of BiOCl nanosheets S5–S8 prepared by solvothermal method with different amount of CTAC as Cl sources under optimal volume ratio of mannitol to EG (1 : 1). Insert pictures are thickness distribution (c) and large magnification of TEM image with scale bar 20 nm (d).

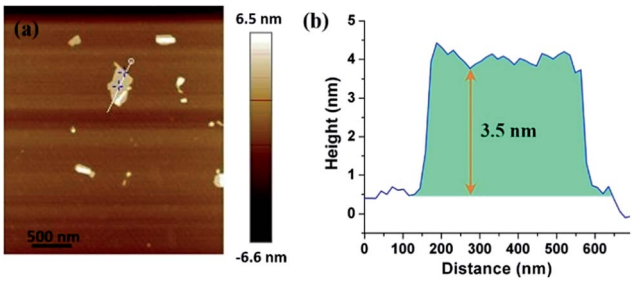

Fig. 3 AFM image of S7 (a) and its corresponding height profile of ultrathin BiOCl nanosheets (b).

with what TEM image shows. Compared with other samples, S5 (Fig. 2a) and S6 (Fig. 2b) have irregular morphologies that resulted from insufficient Cl source. We also investigated the effect of excessive Cl source and obtained S8 (Fig. 2d). The thickness increased from 3–7 nm to 6–13 nm and width could be as large as 72 nm. Thus, under the condition of higher Cl source concentration, the width of nanosheets grows fast and thickness increases largely. Additionally, both S2 and S7 were prepared under optimal volume of solvents and amount of Cl source (NaCl and CTAC, respectively). When we study their morphology shown in TEM images, S7 is square-like while S2 is round square.

3.4. BET and XRD analysis

Specific surface area is considered to be one important aspect when evaluating a good candidate for photocatalytic application. As shown in Fig. 4, BET specific surface areas of S2 and S7 were investigated by nitrogen adsorption–desorption measurements. The BET surface areas of S2 and S7 calculated from the results of nitrogen adsorption are 35.2 and 20.8 $m^2\ g^{-1}$, respectively. Compared with the reported surface areas of commercial BiOCl powder, which is 0.2 $m^2\ g^{-1}$,[9] S2 and S7 are 170 times and 100 times larger, respectively. These values are also larger than other reported values (8.1 $m^2\ g^{-1}$ from Chen's group;[9] 4.8 $m^2\ g^{-1}$ from Zhang's group[10]). The larger BET surface area is expected to enhance higher photocatalysis efficiency. It also indicates that with same optimal parameters except different Cl source, BiOCl nanosheets prepared by using NaCl have larger surface areas than the ones prepared by using CTAC.

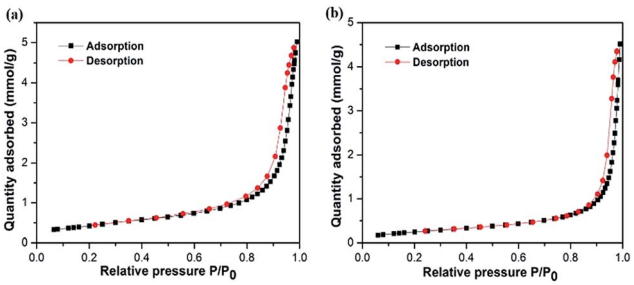

Fig. 4 Nitrogen adsorption–desorption isotherms of S2 (a) and S7 (b).

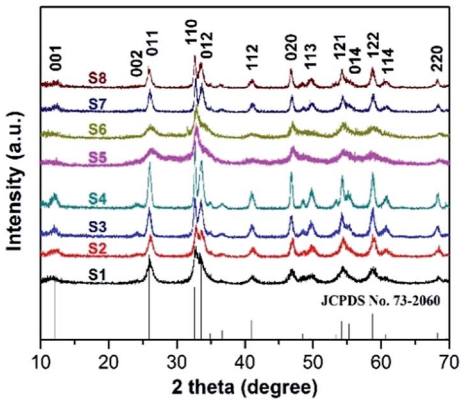

Fig. 5 XRD patterns of BiOCl S1–S8 under various preparation conditions.

The crystallinity of all as-prepared samples were tested by powder XRD analysis. Fig. 5 reveals the typical XRD patterns of BiOCl samples 1–8 synthesized in different conditions. From the XRD results we obtained, the diffraction peaks occurring at 12.0°, 25.9°, 32.6°, 33.6°, 41.0°, 46.8°, 49.9°, 54.2°, 55.3° and 58.8° are readily indexed as (001), (011), (110), (012), (112), (020), (113), (121), (014) and (122) facets, being consistent with tetragonal BiOCl structure (JCPDS 73-2060). There are no other diffraction peaks observed in this pattern, which indicates that the purity of product BiOCl is high. In our experiments, the formation of BiOCl ultrathin nanosheets are no doubt relevant to the coordination interaction between solvents and precursors. The volume ratio between EG and mannitol solution determines the structure and morphology of products, but without changing the product's crystal phase. Among them, sample 2, 3, 4, 7, 8 with sharp and intense diffraction peaks suggests that those as-synthesized samples were well-crystallized. As we know, high crystalline quality and purity are considered to be important factors influencing the photocatalytic activity.[9] Among S5–S7, with optimal experiment parameters (Bi : Cl = 1 : 1), we considered S7 was well-synthesized with good quality of crystalline. It also could be verified from TEM images: S7 shows comparably uniform square-like morphology and narrow width distribution.

3.5. Photocatalytic performances and mechanism

The visible-light-driven photocatalytic efficiency of the BiOCl samples were evaluated by degradation of RhB dye solution. Fig. 6 displays the variation in concentration of RhB (C/C_0) with light irradiation time over various sample photocatalysts, where C is the concentration of RhB at time t and C_0 is its initial concentration. From Fig. 6a, it is clearly observed that S2 exhibits the highest photocatalytic activity when making a comparison of S1, S2 and S3. The RhB solution could be degraded about 97% within 20 min. Thus, this optimal volume ratio condition resulted in a highly efficient photocatalyst. In Fig. 6b, it is noticeable that S7 shows the fastest degradation rate and RhB dye was degraded completely after 20 min. Compared with S5, S7 shows better performance in photocatalysis. It could be attributed to

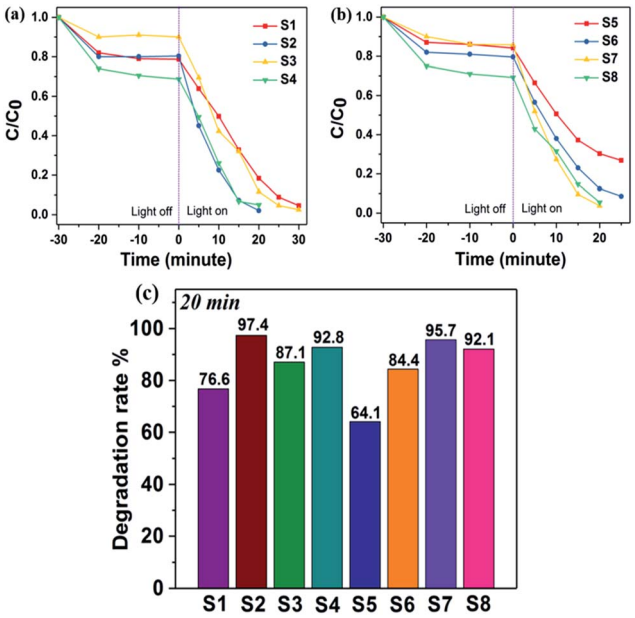

Fig. 6 Concentration ratio of RhB with irradiation time before and after dark adsorption equilibration (a and b), and comparative studies of RhB degradation rate over photocatalysts S1–S8 (c).

higher crystalline quality and more uniform morphology of S7, which was obtained with optimal experiment parameters. The comparison of degradation rates among S1–S8 were indicated in Fig. 6c. We can conclude that with ultrathin and uniform morphology, the photocatalysis efficiency of BiOCl nanosheets could be highly enhanced. S2 and S7 were prepared with optimal experiment conditions and they completed the degradation the most rapidly (97.4% and 95.7%, respectively), which matches our prediction. S4 and S8, which have both larger thickness and width comparably, were synthesized under the condition of excessive Cl source. The degradation rates for S4 and S8 are 92.8% and 92.1%, respectively. As far as we know, these ultrathin BiOCl nanosheets prepared in our method have comparably higher photocatalysis activity than most reported BiOCl materials with similar morphology such as larger nanoplates[8,9] and hierarchical microspheres.[11,12,25] The main factor which leads to improvement of photocatalysis efficiency is larger surface area, that not only harvesting light well, but also providing more efficient transport for charge carriers and promoting diffusion of reactants.[25] The stability of BiOCl nanosheets was further

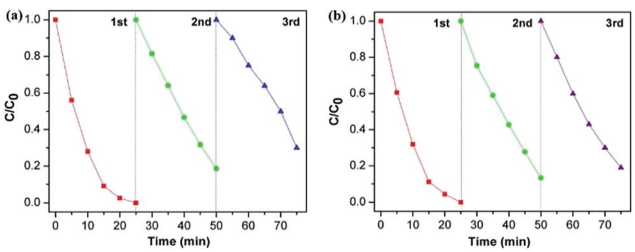

Fig. 7 Recycling test for RhB (10^{-5} M, 20 mL) degradation over 10 mg photocatalysts S2 (a) and S7 (b) under irradiation of visible light.

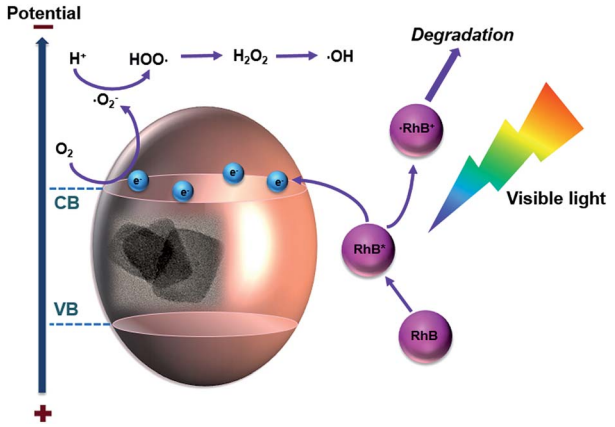

Scheme 2 Schematic mechanism of RhB solution photodegradation under visible-light irradiation.

explored by recycling tests on photodegradation of RhB, choosing S2 and S7 as examples. As shown in Fig. 7, the results indicate that visible-light-driven photocatalytic activity remains relatively consistent over three cycles. The ultrathin BiOCl nanosheets have a good cycling performance, which is beneficial to practical applications.

Scheme 2 illustrates the proposed mechanism of BiOCl photodegradation of RhB with visible-light irradiation. Because of a wide band gap of BiOCl, which is about 3.25 eV, it is negligible to degrade RhB through a direct photocatalytic pathway.[5,9] It is probable that BiOCl proceeds a superior activity *via* a photosensitization pathway, where RhB molecules act as photosensitizer.[30,32] In this case, BiOCl plays a critical role as the carrier and acceptor of electrons. As shown in Scheme 2, BiOCl nanosheets are not able to absorb visible light energy directly; instead, they absorb RhB molecules. RhB adsorbs light energy to produce singlet and triplet states as well as to provide the electron injection into the conduction band (CB) of BiOCl, which lead to conversion of RhB molecule to cation $^{\cdot}RhB^{+}$ and forms BiOCl (e^{-}).[33] After that, BiOCl (e^{-}) reacts with the surface-adsorbed O_2 and produce reactive oxygen radicals which contains radical $^{\cdot}O_2^{-}$ and $^{\cdot}OH$. The $^{\cdot}RhB^{+}$ finally reacts with reactive oxygen to produce degraded products.[33]

4. Conclusions

In summary, we successfully synthesized uniform ultrathin BiOCl nanosheets with high yields *via* a facile solvents co-mediated solvothermal method. We discussed what the crucial roles that polyols and Cl sources might play in preparing BiOCl nanostructures. The thickness of nanosheets were tuned by adjusting volume ratio of solvents as well as concentration of Cl sources. With optimal volume ratio of solvents, we obtained square-like ultrathin BiOCl nanosheets with large surface area, which exhibit excellent visible-light photocatalytic activity for dye degradation. According to the possible mechanism of crystal growth we proposed, further work will be focused on preparation of other bismuth oxyhalides and their composites, for example, BiOBr and BiOI.

Acknowledgements

This study was supported by a startup fund of Washington State University (WSU), USA. We thank Professor Ping Yang from University of Jinan, China for helpful discussion during the research and manuscript preparation. We thank Professor Ming Xian from Department of Chemistry (WSU) and Dr Wei Chen for tests of photodegradation with the Thermo Scientific Evolution 300 UV-vis spectrometer. We thank Franceschi Microscopy & Image Center at WSU for all TEM tests.

Notes and references

1 A. Mills, R. H. Davies and D. Worsley, Water purification by semiconductor photocatalysis, *Chem. Soc. Rev.*, 1993, **22**, 417–425.
2 H. Li, J. Liu, W. Hou, N. Du, R. Zhang and X. Tao, Synthesis and characterization of g-C_3N_4/Bi_2MoO_6 heterojunctions with enhanced visible light photocatalytic activity, *Appl. Catal., B*, 2014, **160**, 89–97.
3 Q. Zhang, J. Wang, D. Xu, Z. Wang, X. Li and K. Zhang, Facile large-scale synthesis of vertically aligned CuO nanowires on nickel foam: growth mechanism and remarkable electrochemical performance, *J. Mater. Chem. A.*, 2014, **2**, 3865.
4 J. Tian, Y. Leng, Z. Zhao, Y. Xia, Y. Sang, P. Hao, J. Zhan, M. Li and H. Liu, Carbon quantum dots/hydrogenated TiO_2 nanobelt heterostructures and their broad spectrum photocatalytic properties under UV, visible, and near-infrared irradiation, *Nano Energy*, 2015, **11**, 419–427.
5 X. Chen and S. S. Mao, Titanium dioxide nanomaterials: synthesis, properties, modifications, and applications, *Chem. Rev.*, 2007, **107**, 2891–2959.
6 H. Cheng, B. Huang and Y. Dai, Engineering BiOX (X = Cl, Br, I) nanostructures for highly efficient photocatalytic applications, *Nanoscale*, 2014, **6**, 2009–2026.
7 L. Ye, Y. Su, X. Jin, H. Xie and C. Zhang, Recent advances in BiOX (X = Cl, Br and I) photocatalysts: synthesis, modification, facet effects and mechanisms, *Environ. Sci.: Nano*, 2014, **1**, 90–112.
8 M. Guan, C. Xiao, J. Zhang, S. Fan, R. An, Q. Cheng, J. Xie, M. Zhou, B. Ye and Y. Xie, Vacancy associates promoting solar-driven photocatalytic activity of ultrathin bismuth oxychloride nanosheets, *J. Am. Chem. Soc.*, 2013, **135**, 10411–10417.
9 J. Xiong, G. Cheng, G. Li, F. Qin and R. Chen, Well-crystallized square-like 2D BiOCl nanoplates: mannitol-assisted hydrothermal synthesis and improved visible-light-driven photocatalytic performance, *RSC Adv.*, 2011, **1**, 1542–1553.
10 J. Jiang, K. Zhao, X. Xiao and L. Zhang, Synthesis and facet-dependent photoreactivity of BiOCl single-crystalline nanosheets, *J. Am. Chem. Soc.*, 2012, **134**, 4473–4476.
11 J. Xiong, G. Cheng, F. Qin, R. Wang, H. Sun and R. Chen, Tunable BiOCl hierarchical nanostructures for high-efficient photocatalysis under visible light irradiation, *Chem. Eng. J.*, 2013, **220**, 228–236.

12 L. Ye, L. Zan, L. Tian, T. Peng and J. Zhang, The {001} facets-dependent high photoactivity of BiOCl nanosheets, *Chem. Commun.*, 2011, **47**, 6951–6953.

13 K. Zhao, L. Zhang, J. Wang, Q. Li, W. He and J. J. Yin, Surface structure-dependent molecular oxygen activation of BiOCl single-crystalline nanosheets, *J. Am. Chem. Soc.*, 2013, **135**, 15750–15753.

14 X. Zhang, X.-B. Wang, L.-W. Wang, W.-K. Wang, L. L. Long, W.-W. Li and H.-Q. Yu, Synthesis of a highly efficient BiOCl single-crystal nanodisk photocatalyst with exposing {001} facets, *ACS Appl. Mater. Interfaces*, 2014, **6**, 7766–7772.

15 Y. Sun and Y. Xia, Large-scale synthesis of uniform silver nanowires through a soft, self-seeding, polyol process, *Nature*, 1991, **353**, 737.

16 P. Toneguzzo, G. Viau, O. Acher, F. Fiévet-Vincent and F. Fiévet, Monodisperse ferromagnetic particles for microwave applications, *Adv. Mater.*, 1998, **10**, 1032–1035.

17 X. Zhang, Z. Ai, F. Jia and L. Zhang, Generalized one-pot synthesis, characterization, and photocatalytic activity of hierarchical BiOX (X = Cl, Br, I) nanoplate microspheres, *J. Phys. Chem. C*, 2008, **112**, 747–753.

18 Z. Cui, L. Mi and D. Zeng, Oriented attachment growth of BiOCl nanosheets with exposed {110} facets and photocatalytic activity of the hierarchical nanostructures, *J. Alloys Compd.*, 2013, **549**, 70–76.

19 J. Xia, S. Yin, H. Li, H. Xu, L. Xu and Y. Xu, Improved visible light photocatalytic activity of sphere-like BiOBr hollow and porous structures synthesized *via* a reactable ionic liquid, *Dalton Trans.*, 2011, **40**, 5249–5258.

20 L. Zhang, X. F. Cao, X. Chen and Z. Xue, BiOBr hierarchical microspheres: microwave-assisted solvothermal synthesis, strong adsorption and excellent photocatalytic properties, *J. Colloid Interface Sci.*, 2011, **354**, 630–636.

21 X. Gao, X. Zhang, Y. Wang, S. Peng, B. Yue and C. Fan, Rapid synthesis of hierarchical BiOCl microspheres for efficient photocatalytic degradation of carbamazepine under simulated solar irradiation, *Chem. Eng. J.*, 2015, **263**, 419–426.

22 D. Wang, G. Gao, Y. Zhang, L. Zhou, A. Xu and W. Chen, Nanosheet-constructed porous BiOCl with dominant {001} facets for superior photosensitized degradation, *Nanoscale*, 2012, **4**, 7780–7785.

23 L. Ye, X. Jin, Y. Leng, Y. Su, H. Xie and C. Liu, Synthesis of black ultrathin BiOCl nanosheets for efficient photocatalytic H_2 production under visible light irradiation, *J. Power Sources*, 2015, **293**, 409–415.

24 D. Zhang, M. Wen, B. Jiang, G. Li and C. Y. Jimmy, Ionothermal synthesis of hierarchical BiOBr microspheres for water treatment, *J. Hazard. Mater.*, 2012, **211**, 104–111.

25 G. Cheng, J. Xiong and F. J. Stadler, Facile template-free and fast refluxing synthesis of 3D desertrose-like BiOCl nanoarchitectures with superior photocatalytic activity, *New J. Chem.*, 2013, **37**, 3207–3213.

26 Y. Wang and Y. Xia, Bottom-up and top-down approaches to the synthesis of monodispersed spherical colloids of low melting-point metals, *Nano Lett.*, 2004, **4**, 2047–2050.

27 Z. A. Peng and X. Peng, Nearly monodisperse and shape-controlled CdSe nanocrystals *via* alternative routes: nucleation and growth, *J. Am. Chem. Soc.*, 2002, **124**, 3343–3353.

28 K. Zhang, C. Liu, F. Huang, C. Zheng and W. Wang, Study of the electronic structure and photocatalytic activity of the BiOCl photocatalyst, *Appl. Catal., B*, 2006, **68**, 125–129.

29 C. Zhang and Y. Zhu, Synthesis of square Bi_2WO_6 nanoplates as high-activity visible-light-driven photocatalysts, *Chem. Mater.*, 2005, **17**, 3537–3545.

30 J. Ma, X. Liu, J. Lian, X. Duan and W. Zheng, Ionothermal synthesis of BiOCl nanostructures *via* a long-chain ionic liquid precursor route, *Cryst. Growth Des.*, 2010, **10**, 2522–2527.

31 M. Shang, W. Wang and L. Zhang, Preparation of BiOBr lamellar structure with high photocatalytic activity by CTAB as Br source and template, *J. Hazard. Mater.*, 2009, **167**, 803–809.

32 Y. Peng, D. Wang, H. Zhou and A. Xu, Controlled synthesis of thin BiOCl nanosheets with exposed {001} facets and enhanced photocatalytic activities, *CrystEngComm*, 2015, **17**, 3845–3851.

33 T. Wu, G. Liu, J. Zhao, H. Hidaka and N. Serpone, Photoassisted degradation of dye pollutants. V. Self-photosensitized oxidative transformation of rhodamine B under visible light irradiation in aqueous TiO_2 dispersions, *J. Phys. Chem. B*, 1998, **102**, 5845–5851.